PHYSICAL REVIEW C **74**, 054607 (2006)

Theoretical study of one-proton removal from ^{15}O

Y. L. Parfenova*
Physique Nucléaire Théorique et Physique Mathématique, CP229, Université Libre de Bruxelles B 1050 Brussels, Belgium

M. V. Zhukov
Fundamental Physics, Chalmers University of Technology, S-41296 Göteborg, Sweden
(Received 15 June 2006; published 21 November 2006)

One-proton removal from ^{15}O at intermediate energies (56*A* MeV) is studied in the eikonal approximation of the Glauber model. The production of the ^{14}N core fragment in the ground and excited states is studied. The calculated proton removal cross section, the ^{15}O interaction cross section, and the longitudinal momentum distribution of the ^{14}N fragments are compared to recent experimental data [H. Jeppesen *et al.*, Nucl. Phys. **A739**, 57 (2004)].

DOI: 10.1103/PhysRevC.74.054607 PACS number(s): 21.60.Gx, 25.60.Dz, 25.60.Gc

I. INTRODUCTION

During the last decade two-proton emitters and proton-rich nuclei, in the vicinity of the proton drip-line, have been the subject of intensive experimental and theoretical studies. In particular the study of a candidate to possess a two-proton halo in the ground state, namely, the Borromean ^{17}Ne nucleus, is of special experimental and theoretical interest (see, for example, discussions in [1–3]). The inherent feature of the halo structure is a relatively small separation energy of a valence nucleon. It reveals itself in a large valence nucleon removal cross section and a narrow core longitudinal momentum (LM) distribution.

In the case of ^{17}Ne, the proton removal cross section, measured at the energy 66*A* MeV on a Be target [2], is relatively large compared to the cluster model ($^{15}\mathrm{O} + p + p$) predictions [3]. At the same time, the measured [2]^{15}O core LM distribution is wider than the calculated one [3]. Both these facts can be attributed to the contribution of a proton removal from the ^{15}O core in ^{17}Ne if this cross section is relatively large (for details, see Ref. [3]).

Recently the ^{14}N longitudinal momentum (LM) distribution and breakup cross section (into the $^{14}\mathrm{N} + p$ channel) have been measured in fragmentation of ^{15}O on a Be target at the energy 56 *A* MeV [4]. This raises the possibility for more precise calculations of the proton removal from ^{17}Ne and evaluations of the contribution of the proton removal from the ^{15}O core to this process.

In this article, we present a detailed analysis of the ^{15}O breakup in light targets. We perform the calculations in the eikonal approximation of the Glauber model [5,8–10]. This approach is well developed and convenient for calculations of breakup cross sections, interaction cross sections, and momentum distributions of fragments in breakup of a nucleus at intermediate and high energies (from 30 to 1000*A* MeV).

The formalism for the calculations is described in Sec. II. The main ingredients of the Glauber model are the wave function of the relative motion of the fragments and the profile functions defining the fragment-target interaction. They are fixed using experimental data on the nucleon-nucleus and nucleus-nucleus cross sections, proton separation energies, the level scheme of the core nucleus, etc. In particular, the profile functions are fitted using the nucleus-nucleus and nucleon-nucleus interaction cross sections.

The wave function is obtained in the core+proton ($^{14}\mathrm{N} + p$) model of ^{15}O, where the ^{14}N core fragment can be in the ground and excited states (see, for example, Ref. [10]). The *p*-wave proton removal from ^{15}O ($J^\pi = 1/2^-$) leads to a few ^{14}N bound states. We consider four of them (for details see [11]): $E_x = 0.0$ MeV ($J^\pi = 1^+, T = 0$), $E_x = 2.313$ MeV ($0^+, 1$), $E_x = 3.948$ MeV ($1^+, 0$), and $E_x = 7.029$ MeV ($2^+, 0$). Here, E_x is the excitation energy and (J^π, T) are the spin and isospin of the ^{14}N state. For each state, the depth of the ($^{14}\mathrm{N} + p$) interaction potential (see, below) is fitted to reproduce the proton separation energy.

The cross sections of the proton removal from the ^{15}O ground state are determined by the spectroscopic factors [11, 12] of the *p*-wave proton states.

In Sec. III we fit the profile functions in calculations of the corresponding nucleus-nucleus and proton-nucleus interaction cross sections and compare results to the available experimental data.

In Sec. IV we present the calculated cross sections and longitudinal momentum distributions of the ^{14}N fragments produced in various states in the process of the one-proton removal from ^{15}O on a ^{9}Be target. These results are compared to the experimental data on the ^{14}N longitudinal momentum distribution and the breakup cross section measured at the energy 56*A* MeV [4].

II. CROSS SECTIONS AND MOMENTUM DISTRIBUTIONS

In the core-nucleon model of the projectile nucleus, the initial state is described by the wave function (WF) $\Psi_{JM_J}(\vec{r})$ of the core-nucleon relative motion with a total angular momentum J and its projection M_J. The WF depends on the relative coordinate $\vec{r}$ between nucleon and core and, also,

*Electronic address: Yulia.Parfenova@ulb.ac.be. Also at Skobeltsyn Institute of Nuclear Physics, Moscow State University, 119992 Moscow, Russia.

on the total angular momentum j_n of the valence nucleon and fragment spins.

After interaction with a target, the WF of the projectile will be corrected by factors connected with nucleon-target and core-target interactions. Thus, the WF in the projectile rest frame is modified as [5]

$$\Psi(\vec{r}, \vec{R}) = S_c(b_c)S_n(b_n)\Psi_{JM_J}(\vec{r}), \tag{1}$$

where $\vec{R}$ is the coordinate of the center of mass of the projectile, $b_i = |\vec{b}_i|$ $(i = n, c)$, and $\vec{b}_n$ and $\vec{b}_c$ are the transverse two-dimensional impact parameters of the nucleon and the core with respect to the target nucleus; i.e., $\vec{b}_n = \vec{R}_\perp + \vec{r}_\perp A_c/(A_c+1)$ and $\vec{b}_c = \vec{R}_\perp - \vec{r}_\perp/(A_c+1)$, where $\vec{R}_\perp$ and $\vec{r}_\perp$ are components, perpendicular to the beam direction taken as z axis, and A_c is the mass number of the core. The profile functions $S_n(b_n)$ and $S_c(b_c)$ are generated by nucleon and core interactions with the target nucleus.

The fragmentation includes nucleon stripping and diffraction processes. The corresponding cross sections are given by the equations [5–7]

$$\sigma_{\rm str} = \frac{1}{2L+1}\sum_M \int d\vec{R}_\perp \int d\,\vec{r}\;\Psi^*_{\rm LM}(\vec{r})\,(1-|S_n|^2) \times |S_c|^2\;\Psi_{\rm LM}(\vec{r})$$

$$\sigma_{\rm diff} = \frac{1}{2L+1}\sum_M \int d\vec{R}_\perp \int d\,\vec{r}\;\Psi^*_{\rm LM}(\vec{r})\,|S_nS_c|^2\;\Psi_{\rm LM}(\vec{r}) - \frac{1}{2J+1}\sum_{M_JM'_J}\int d\vec{R}_\perp \left|\int d\,\vec{r}\;\Psi^*_{JM'_J}(\vec{r})\,S_nS_c \times \Psi_{JM_J}(\vec{r})\right|^2. \tag{2}$$

The proton removal cross section is found as the sum $\sigma_{-p} = \sigma_{\rm str} + \sigma_{\rm diff}$. The wave function Ψ_{JM_J} is

$$\Psi_{JM_J} = [[\Psi_{\rm LM}(\vec{r}) \otimes \chi_{s_nm_n}]_{j_n} \otimes \chi_{s_cm_c}]_{JM_J}, \tag{3}$$

where $\chi_{s_cm_c}$ is the internal wave function of the core including the spin function and $\chi_{s_nm_n}$ is the spin function of the valence nucleon.

We denote the part of the WF related to the relative motion as $\Psi_{\rm LM}$

$$\Psi_{\rm LM}(\vec{r}) = R_L(r)Y_{\rm LM}, \tag{4}$$

where $Y_{\rm LM}$ is the spherical function.

The radial part of the core-proton WF, $R_L(r)$, is obtained as a solution of the Schrödinger equation for the Woods-Saxon potential (the Coulomb ^{14}N $+\,p$ potential is also included). For each state of ^{14}N, the parameter V_0 of the Woods-Saxon potential is fitted to reproduce the proton separation energy with the fixed parameters $a_0 = 0.65$ fm and $R_0 = 1.25A^{1/3} = 3.00$ fm. The depth parameters and the proton separation energies are given in Table I.

In the calculations of the cross sections and LM distributions of the fragments we consider the p ($p_{1/2}$ and $p_{3/2}$) proton removal. The p-wave proton removal from ^{15}O leads to the residual ^{14}N core in the bound states $E_x = 0.0$ MeV ($J^\pi = 1^+, T = 0$), $E_x = 2.313$ MeV (0^+, 1), $E_x = 3.948$ MeV (1^+, 0), and $E_x = 7.029$ MeV (2^+, 0).

TABLE I. The depth parameter V_0 of the Woods-Saxon potential, obtained with the diffuseness parameter $a_0 = 0.65$ fm and radius $R_0 = 3.00$ fm for the p-wave proton separation energy E_s. E_x is the corresponding ^{14}N core excitation energy. C^2S are the spectroscopic factors.

E_x (MeV)	^{14}N (J^π, T)	C^2S[a]	C^2S[b]	Woods-Saxon potential	
				V_0 (MeV)	E_s (MeV)
0	$(1^+, 0)$	1.459	1.343	−48.09	7.297
2.313	$(0^+, 1)$	0.418	0.472	−52.07	9.610
3.948	$(1^+, 0)$	0.696	0.656	−54.78	11.245
7.029	$(2^+, 0)$	1.250	1.250	−59.73	14.326

[a]Reference [12].
[b]Reference [14].

Note, that the spectroscopic factors are not measured yet for ^{15}O. As was shown in the distorted wave Born approximation (DWBA) analysis [13], the contribution of the protons with $l = 1$ dominates in the proton transfer reaction leading to the ground state of ^{15}O. The spectroscopic factors of the states can be taken as those predicted by Cohen and Kurath [12]. These values are close to the measured values in the neutron pick-up reactions with the mirror ^{15}N nucleus, the ^{15}N$(p,d)^{14}$N reaction with 40 MeV protons [11], and the ^{15}N$(d,t)^{14}$N reaction with 90 MeV deuterons [14] (see the discussion in Ref. [4] and references therein). We use the spectroscopic factors from Refs. [12] and [14]. These factors C^2S are also listed in Table I.

Note, that the contribution of the ^{15}O excited bound states to the last term in expression (2) for the diffraction cross section is neglected here.

The LM distributions of the core fragments are obtained by the Fourier transformation of the core-proton WF, $R_L(r)$, corrected for the core-target and nucleon-target interactions

$$\frac{d\sigma_{\rm str}}{dk_z} = \frac{1}{2L+1}\int_0^\infty b_n db_n (1-|S_n(b_n)|^2) \times \int_0^\infty r_\perp dr_\perp d\phi |S_c(|\vec{b}_n - \vec{r}_\perp|)|^2 \times \sum_M \left|\int_{-\infty}^\infty e^{ik_zz} R_L\left(\sqrt{r_\perp^2+z^2}\right)Y_{\rm LM}dz\right|^2. \tag{5}$$

The core longitudinal momentum distribution in the diffraction breakup is assumed to be similar [5,15] to that of stripping.

Equation (5) gives the contribution of the LM distribution coming from each neutron-core state composing the ^{15}O ground state wave function. For comparison with the experimental data, we sum up these contributions weighted by the spectroscopic factors (Table I).

The fragment-target interaction cross section is determined by the profile function $S_\nu(\vec{b}_\nu)$ as

$$\sigma_I^\nu = \int d^2\vec{b}_\nu\,(1-|S_\nu(\vec{b}_\nu)|^2), \tag{6}$$

where index ν denotes the fragment ($\nu = p, ^{14}$N) and $\vec{b}_\nu$ is the impact parameter of the νth fragment.

The interaction cross section for the fragmented projectile is expressed through the profile functions of the fragment-target interaction and the wave function of the relative motion of the fragments.

$$\sigma_I = \frac{1}{2J+1} \sum_{M_J} \int d\vec{R}_\perp \times \left[1 - \sum_{M'_J} \left| \int d\,\vec{r}\; \Psi^*_{JM'_J}(\vec{r})\; S_n S_c\; \Psi_{JM_J}(\vec{r}) \right|^2 \right]. \quad (7)$$

III. PROFILE FUNCTIONS

The profile function of the fragment-target interaction in Eqs. (1), (2), and (5) is determined as an integral of the corresponding complex interaction potential

$$S_\nu(\vec{b}_\nu) = \exp\left[-\frac{i}{\hbar v} \int_{-\infty}^{\infty} dz\;\; V_{\nu T}\left(\sqrt{b_\nu^2 + z^2}\right) \right], \quad (8)$$

where $V_{\nu T}(r)$ is the fragment-target interaction potential and v is the ^{15}O beam velocity in the laboratory frame. The fragment-target interaction potential is determined by folding of the fragment density distribution and the nucleon-target interaction potential.

To calculate the nucleon-target interaction potential $V_{\nu T}(r)$ ($\nu = n, p$) at energies less than 65A MeV, we use the parameters of the global nucleon-nucleus optical potential [16]. We also use the interaction potential [5] generated from the free nucleon-nucleon (*NN*) interaction [17,18] valid at energies from 10 to 2000A MeV. In this case, the nucleon-target interaction potential is obtained by folding of the target density distribution and the nucleon-nucleon interaction potential. For the details of the profile function calculations we refer the reader to Refs. [6,10].

For description of the target and fragment nuclear densities we use different parametrizations. The ^{9}Be and ^{14}N densities are parameterized in the harmonic oscillator model [19]

$$\rho(r) = \rho_0[1 + \alpha(r/a)^2]\exp(-(r/a)^2)\,. \quad (9)$$

The parameter α is related to a [19]. The parameter α is fitted (see Sec. IV) to reproduce nucleon-nucleus and nucleus-nucleus interaction cross sections.

The ^{12}C density distribution is approximated by a sum of Gaussians [19] as

$$\rho(r) = \sum_i A_i\left(e^{-(r-\beta R_i)^2/\gamma^2} + e^{-(r+\beta R_i)^2/\gamma^2}\right), \quad (10)$$

with the parameters from Ref. [19]. To vary the calculated cross section obtained with the density distribution (10), we introduce a scaling factor β and replace R_i by βR_i in Eq. (10).

All the distributions ρ are normalized to unity, and ρ_0 is a normalization factor.

To fit the profile functions, corresponding experimental data for interaction (reaction) cross sections on C and Be targets at intermediate and high energies are used.

In the case of ^{12}C, the scaling parameter β in Eq. (10) is fitted to reproduce the experimental data for ^{12}C + ^{12}C [20–29] and $p + {}^{12}$C [29,30] interaction cross sections. The best fit is achieved for $\beta = 0.94$. With this β value the ^{12}C rms radius is 2.37 fm, which is close to the ^{12}C rms matter radius 2.33 fm obtained in Ref. [20].

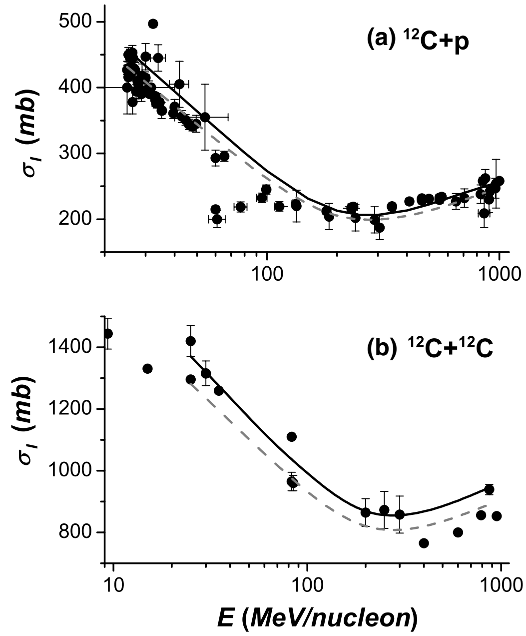

FIG. 1. (Color online) The energy dependence of the $p + {}^{12}$C and ^{12}C + ^{12}C interaction cross sections, σ_I, calculated with the NN interaction potential. The solid circles in (a) and (b) represent the experimental data from [29,30] and [20–29], respectively. The curves correspond to $\beta = 0.94$ (dashed gray lines) and $\beta = 1$ (solid black lines).

Figures 1(a) and 1(b) show the calculated (dashed gray curves) and measured (dots) $p + {}^{12}$C and ^{12}C + ^{12}C interaction cross sections at energies from 20 to 1000A MeV. For comparison, the cross sections obtained with the charge radius of carbon $r_c = 2.47$ fm ($\beta = 1$) are also given in Fig. 1 (solid black curves).

The ^{9}Be density parameter a in Eq. (9) is fitted to reproduce the experimental data on the $p + {}^9$Be [29,30] and ^{9}Be + ^{9}Be [24] interaction cross sections. The value $a = 1.69$ fm corresponds the ^{9}Be rms radius 2.38 fm [20]. To have a measure of sensitivity of the results to the input parameters of the model, we present the results of the calculations with the parameter $a = 1.79$ fm, also allowing a good fit of the ^{9}Be nucleus cross section.

In Figs. 2(a) and 2(b) the calculated cross sections are compared to the experimental data. These results are also compared to the calculations with the Be rms radius equal to the Be charge radius, 2.52 fm ($a = 1.79$ fm) [19].

The $p + {}^9$Be interaction cross section calculated with the NN interaction potential at energies less than 60A MeV is underestimated, while that obtained with the optical model potential satisfy the experimental data. At higher energies, the cross section calculated with the NN interaction potential is in a good agreement with the experimental data [29].

To test the fitted density parameters of ^{12}C and ^{9}Be we calculate the interaction cross section in the ^{9}Be + ^{12}C reaction

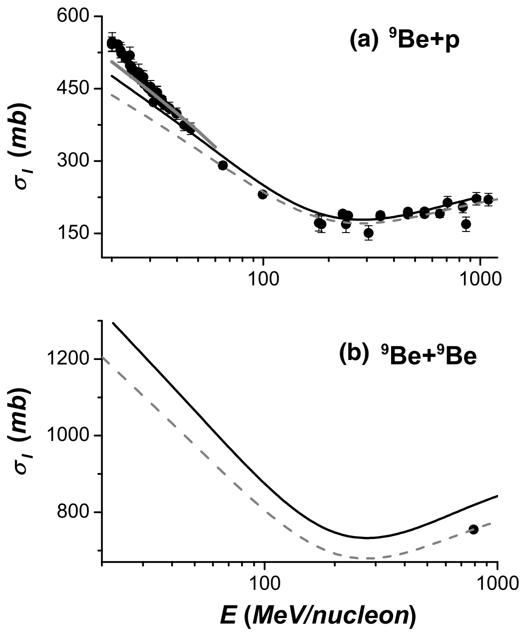

FIG. 2. (Color online) The energy dependence of the $p + {}^9$Be and ^{9}Be + ^{9}Be interaction cross sections, σ_I. The solid circles in (a) and (b) represent the experimental data from Refs. [29,30] and [24], respectively. Dashed gray and solid black lines are the calculations with the NN interaction potential with the parameters $a = 1.69$ and $a = 1.79$ fm, respectively. The solid grey line represents the calculations with the optical model potential (OMP).

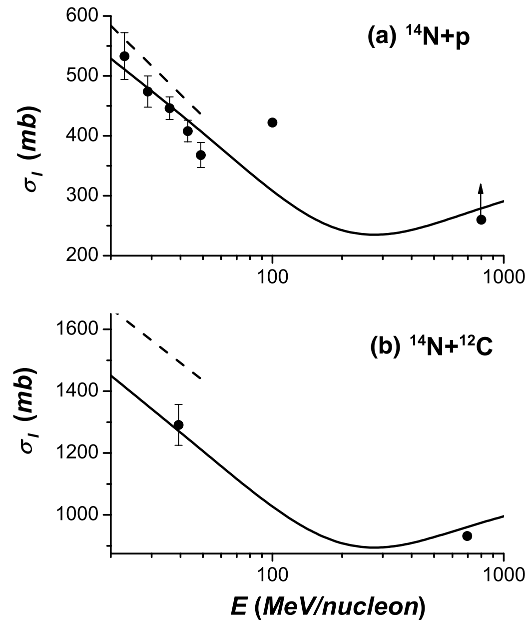

FIG. 3. The energy dependence of the $p + {}^{14}$N and ^{14}N + ^{12}C interaction cross sections, σ_I. The solid circles in (a) and (b) represent the experimental data from [29,30] and [20,31], respectively. The calculations with the NN interaction potential and the OMP are shown by solid and dashed lines, respectively.

at the energy 790A MeV. The value, 818.7 mb, is very close to the experimental one 806(9) mb [20].

Using the experimental data on the ^{14}N + p reaction [29] and the ^{14}N + ^{12}C reaction at the energies 39.3 [31] and 965A MeV [20], we found $a = 1.76$ fm in the ^{14}N density parametrization (9). This value corresponds to the ^{14}N rms matter radius 2.44 fm known from experiment.

The results of these calculations and the experimental data are given in Fig. 3. The cross sections calculated with the NN interaction potential are in a better agreement with the experimental data for both the proton-nucleus and the nucleus-nucleus interaction cross sections than those obtained with the optical model potential.

For further calculations of the ^{15}O breakup on a Be target at the energy 56A MeV we use profile functions obtained with the NN interaction potential.

With the ^{14}N rms radius we can estimate the ^{15}O rms radius as

$$r_m^2({}^{15}\mathrm{O}) = \frac{A_c A_p}{A^2}\langle r_{c-p}^2\rangle + \frac{A_c}{A} r_m^2({}^{14}\mathrm{N}), \tag{11}$$

where r_{c-p} is the distance of the valence proton from the ^{14}N center of mass, $A = A_c + A_p$ is the mass number of the projectile, and the valence proton mass number $A_p = 1$.

With the ^{14}N rms matter radius $r_m = 2.44$ fm, which corresponds ($r_c^2 = r_m^2 + 0.8^2$) to the charge radius $r_c({}^{14}\mathrm{N}) =$ 2.57 fm [19], and the rms r_{c-p} distance of the proton $\langle r_{c-p}^2\rangle^{\frac{1}{2}} = 3.15$ fm, the ^{15}O rms matter radius is $r_m({}^{15}\mathrm{O}) =$ 2.48 fm. This value is consistent with the values obtained in Refs. [20,32]. The corresponding ^{15}O rms charge radius is $r_c({}^{15}\mathrm{O}) = 2.61$ fm.

In Table II, the values of the ^{15}O interaction cross section (7) obtained in the ^{12}C and ^{9}Be targets with the fitted density parameters are compared to the experimental data. One can see a good agreement with the experimental data [20].

IV. RESULTS AND DISCUSSION

The ^{14}N and ^{15}O interaction cross sections obtained at the energy 56A MeV on a Be target are $\sigma_I({}^{14}\mathrm{N}) = 1061$ mb and $\sigma_I({}^{15}\mathrm{O}) = 1091$ mb, respectively.

One-proton removal cross sections from ^{15}O and the corresponding full width at half maximum (FWHM) values of the LM distribution of the ^{14}N fragments obtained at the energy 56A MeV for a Be target are listed in Table III. All the

TABLE II. The calculated (σ_I) and measured (σ_I^{exp}) nucleus-nucleus interaction cross sections.

Projectile	Target	E (MeV/nucleon)	σ_I (mb)	σ_I^{exp} (mb)
^{15}O	^{9}Be	710	881[a]	912(23)
	^{9}Be	710	920[b]	
	^{12}C	670	939	915(13)
	^{12}C	710	945	922(49)

[a]Obtained with $a = 1.694$ fm.
[b]Obtained with $a = 1.791$ fm.

TABLE III. The single-particle one-proton removal cross section ($\sigma_{-p}^{\rm sp}$) and the one-proton removal cross section (σ_{-p}) from ^{15}O calculated at the energy 56*A* MeV on a Be target.

^{14}N (J^π, T)	$\sigma_{-p}^{\rm sp}$ (mb)	σ_{-p} (mb)	FWHM (MeV/c)
(1^+, 0)	29.7	43.3	178
(0^+, 1)	25.9	10.8	191
(1^+, 0)	23.3	16.2	198
(2^+, 0)	20.4	25.6	209
Total		95.9	191

values are calculated with the Be target density parameter $a =$ 1.69 fm. The single-particle proton removal cross sections, $\sigma_{-p}^{\rm sp}$, and those multiplied by the corresponding spectroscopic factors [12], σ_{-p}, are given for each single-particle state.

The total value of the one-proton removal cross section and the LM distribution (last row of Table III) is found as the sum of the proton removal cross sections σ_{-p} and the corresponding LM distributions.

The calculated values of the total proton removal cross section and the FWHM (Table III) obtained with the Be target density parameter $a = 1.69$ fm and the spectroscopic factors [12] are in very good agreement with the experimental values 80 ± 20 mb and 190 ± 10 MeV/c [4]. With the spectroscopic factors from Ref. [14] the value of the proton removal cross section is 92.0 mb. With the larger target density parameter $a = 1.79$ fm, we get larger values of the cross sections. In this case, the total proton removal cross section obtained with the spectroscopic factors [12] is $\sigma_{-p} = 100.2$ mb. So one can see that the total one-proton removal cross section is not very sensitive to small variations of spectroscopic factors or the target density parameter.

In Fig. 4 the calculated LM distributions are compared to the experimental ones [4]. Note, that the theoretical curves are shifted by 10 MeV/c to the left to be compared to the experimental data.

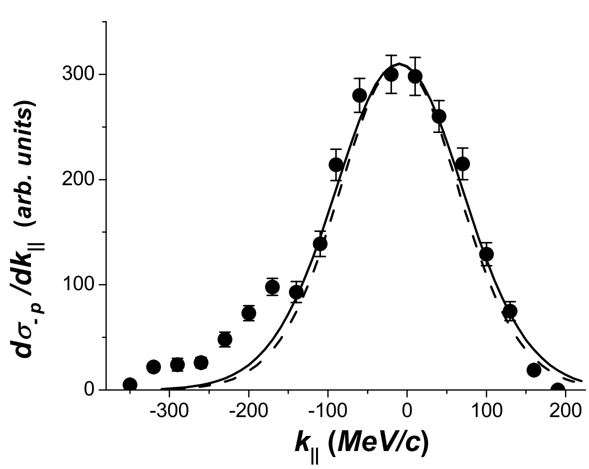

FIG. 4. Total longitudinal momentum distribution of the ^{14}N fragments (solid line) from the ^{15}O breakup on Be target at the energy 56*A* MeV. The solid circles represent the experimental data from Ref. [4]. The dashed line shows the longitudinal momentum distribution of the ^{14}N in the ground state.

The solid line in the figure shows the total LM distribution obtained with all ^{14}N states shown in Table III. The dashed line represents the LM distribution from proton removal leading to ^{14}N in the ground state. As it corresponds to the smaller proton separation energy (Table II), the LM distribution is narrower than that for other ^{14}N states. Thus, the FWHM value of the total LM distribution is larger than that for the ^{14}N ground state by 13 MeV/c.

The consideration of the ^{14}N production in the excited states does not change significantly the LM distribution because each ^{14}N state (including the ground state) is characterized by relatively high proton separation energy and, hence, has nearly the same (Table III) LM distributions. Thus, the value of FWHM is weakly sensitive to the weights of the ^{14}N states and the ^{14}N excitation. However, these contributions are essential in the calculations of the proton removal cross section.

V. CONCLUSION

In this article, we present calculations of the one-proton removal cross sections from ^{15}O on a Be target at the energy 56*A* MeV. The proton removal cross sections, the ^{15}O interaction cross section, and the longitudinal momentum distribution of the ^{14}N fragments are obtained in the eikonal approximation of the Glauber model with the NN interaction potential. In the calculations, the production of the ^{14}N core fragment in the ground and excited states is considered. The calculated FWHM=191 MeV/c of the total LM distribution is very close to the experimentally measured value of 190 ± 10 MeV/c [4].

The calculated value, 95.9 mb, of the total one-proton removal cross section is also very close to the experimental value 80 ± 20 mb [4]. The breakup cross section is about 11% of the ^{15}O interaction cross section.

Returning to the ^{17}Ne problem, we see that the contribution of the proton removal from the ^{15}O core might be essential. In particular, at the energy 66*A* MeV (see experimental data [2]), we get the cross section of the proton removal from the core fragment 94.4 mb. Because of the weakly bound protons blocking the ^{15}O core in ^{17}Ne, this cross section is reduced, contributing about 51 mb to the total one-proton removal cross section. The contribution of the valence proton removal in ^{17}Ne with the spectacular ^{15}O core is about 110 mb [3]. Thus, the calculated total proton removal cross section will be 161 mb. This value satisfies the experimental one, 168 ± 17 mb [2]. Note, that the contribution of the proton removal from the ^{15}O core affects also the width of the total ^{15}O LM distribution.

As a result, in the reactions with ^{17}Ne, the proton removal cross section measured at the energy 66*A* MeV on a Be target [2] is relatively large compared to the cluster model (^{15}O + $p + p$) predictions [3] and the measured ^{15}O LM distribution is wider than the calculated one.

Therefore, the proton removal from the core should necessarily be taken into account in calculations of the ^{17}Ne fragmentation.

[1] M. V. Zhukov and I. J. Thompson, Phys. Rev. C **52**, 3505 (1995).
[2] R. Kanungo, M. Chiba, S. Adhikari *et al*., Phys. Lett. **B571**, 21 (2003); R. Kanungo, Nucl. Phys. **A738**, 293 (2004).
[3] L. V. Grigorenko, Yu. L. Parfenova, and M. V. Zhukov, Phys. Rev. C **71**, 051604(R) (2005).
[4] H. Jeppesen, R. Kanungo, B. Abu-Ibrahim *et al*., Nucl. Phys. **A739**, 57 (2004).
[5] K. Hencken, George Bertsch, and H. Esbensen, Phys. Rev. C **54**, 3043 (1996).
[6] Yu. L. Parfenova and M. V. Zhukov, Phys. Rev. C **66**, 064607 (2002).
[7] J. A. Tostevin, J. Phys. G: Nucl. Part. Phys. **25**, 735 (1999).
[8] H. Esbensen and G. F. Bertsch, Phys. Rev. C **59**, 3240 (1999).
[9] H. Esbensen and K. Hencken, Phys. Rev. C **61**, 054606 (2000).
[10] Yu. L. Parfenova, M. V. Zhukov, and J. S. Vaagen, Phys. Rev. C **62**, 044602 (2000).
[11] J. L. Snelgrove and E. Kashy, Phys. Rev. **187**, 1259 (1969).
[12] S. Cohen and D. Kurath, Nucl. Phys. **A101**, 1 (1967).
[13] J. Bommer, H. Fuchs, K. Grabisch, U. Janetzki, and G. Roschert Nucl. Phys. **A172**, 618 (1971).
[14] S. K. Saha, W. W. Daehnick, S. A. Dytman, P. C. Li, J. G. Hardie, G. P. A. Berg, C. C. Foster, W. P. Jones, D. W. Miller, and E. J. Stephenson, Phys. Rev. C **40**, 39 (1989).
[15] F. Negoita, C. Borcea, F. Carstoiu *et al*., Phys. Rev. C **59**, 2082 (1999).
[16] R. L. Varner, W. J. Thompson, T. L. Mcabee, E. J. Ludwig, and T. B. Clegg, Phys. Rep. **201**, 57 (1991).
[17] S. K. Charagi and S. K. Gupta, Phys. Rev. C **41**, 1610 (1990).
[18] L. Ray, Phys. Rev. C **20**, 1857 (1979).
[19] H. de Vries, C. W. de Jager, and C. de Vries, At. Data Nucl. Data Tables **36**, 495 (1987).
[20] A. Ozawa, T. Suzuki, and I. Tanihata, Nucl. Phys. **A693**, 32 (2001).
[21] C. -C. Sahm, T. Murakami, J. G. Cramer, A. J. Lazzarini, D. D. Leach, D. R. Tieger, R. A. Loveman, W. G. Lynch, M. B. Tsang, and J. VanderPlicht, Phys. Rev. C **34**, 2165 (1986).
[22] W.-Q. Shen *et al*., Nucl. Phys. **A491**, 130 (1989).
[23] Y.-B. Wei, X.-Z. Cai, W.-Q. Shen *et al*., Chin. Phys. Lett. **20**, 354 (2003).
[24] I. Tanihata, H. Hamagaki, O. Hashimoto, Y. Shida, N. Yoshikawa, K. Sugimoto, O. Yamakawa, T. Kobayashi, and N. Takahashi, Phys. Rev. Lett. **55**, 2676 (1985).
[25] S. Kox, A. Gamp, C. Perrin *et al*., Phys. Lett. **B159** 15 (1985).
[26] S. Kox, A. Gamp, C. Perrin *et al*., Phys. Rev. C **35** 1678 (1987).
[27] J. Jaros, A. Wagner, L. Anderson *et al*., Phys. Rev. C **18**, 2273 (1978).
[28] I. Tanihata *et al*., *Radioactive Nuclear Beams,* edited by W. D. Meyers, J. M. Nischke, and E. B. Norman (World Scientific, Singapore, 1990), p. 249.
[29] V. S. Barashenkov in *Secheniya vzaimodeistviya chastits i yader s yadrami* (JINR, Dubna, 1993).
[30] National Nuclear Data Center, http://nndc.bnl.gov (NNDC), Brookhaven National Laboratory, Experimental Nuclear Reaction Data (EXFOR / CSISRS).
[31] D. Q. Fang, W. Q. Shen, J. Feng *et al*., Phys. Rev. C **61**, 064311 (2000).
[32] R. E. Warner, F. Carstoiu, J. A. Brown *et al*., Phys. Rev. C **74**, 014605 (2006).